SCIENCE CHINA
Information Sciences

• **Supplementary File** •

Robustness of interdependent networks with weak dependency links and reinforced nodes

Qian LI, Hongtao YU*, Weitao HAN, Ruiyang HUANG, Shaomei LI & Jianpeng ZHANG

Institute of Information Technology, PLA Strategic Support Force Information Engineering University, Zhengzhou 450000*, China*

Appendix A WD-RN model

Appendix A.1 Topology of the model

Without loss of generality, in Figure A1, our model composes of two fully interdependent sub-networks A and B with degree distributions $p_A(k)$ and $p_B(k)$, respectively, containing the same N nodes. Each node i $(i = 1, 2, ...N)$ has k connectivity links. A node in a sub-network A depends on one and only one node in sub-network B by a weak dependency link, and vice versa, with the no-feedback condition [1]. Here, a weak dependency link structurally means that when a node i (j) in sub-network A (B) fails, each connectivity link of its dependency partner j (i) in sub-network B (A) is disconnected from its neighbor nodes with a probability $1 - \alpha_B$ $(1 - \alpha_A)$, where the parameters α_A and α_B are applied to measure node-dependence strength between networks. When the parameters $\alpha_A \to 0$ and $\alpha_B \to 0$ signifies the maximal strength of the interdependence between sub-networks, and our model is simplified to the original model proposed in [1]. Conversely, When $\alpha_A \to 1$ and $\alpha_B \to 1$, the failures cannot propagate though a weak dependency link between networks, and then our model is reduced to the previous ordinary percolation of the single-layer network with reinforced nodes in [1]. We randomly choose a fraction ρ_A and ρ_B of nodes as reinforced nodes in each sub-network, respectively. These reinforced nodes can maintain function of the finite components in which they are located, even if they are disconnected from the mutual giant (largest) connected component (MGCC). In interdependent networks, these finite components containing at least one reinforced node and the MGCC constitute the mutual generalized giant connected component(MGGCC). Thus, the size of the MGGCC is usually significantly larger than the size of the MGCC, as shown in Figure A2.

Appendix A.2 Failure Mechanism of the model

In Figure A1, a cascading failure process is illustrated in interdependent networks with weak dependency links and reinforced nodes (WD-RN). In our model, the initial random removal of nodes from sub-networks will trigger a series of iterations of connection and dependency failures, named cascading failure. With the failure propagation between sub-networks A and B, the sub-network is fragmented into several components. Divided into several components, those finite components without reinforcement nodes are removed. This process is repeated until an equilibrium state is achieved. Here, Algorithm A1 shows the detailed process of our simulation.

Appendix B Solving general interdependent networks

Appendix B.1 Probabilistic formalization

The proposed model is solved by a series of self-consistent equations based on generating functions [1, 8]. In each sub-network, the generating functions of degree distribution and the associated branching processes are $G_0(x) = \sum_k p(k) x^k$ and $G_1(x) = \sum_k \frac{p(k)k}{\langle k\rangle} x^{k-1}$, where $p(k)$ is degree distribution and $\langle k\rangle$ is the average degree in each sub-network.

Then, we denote f as the probability that a randomly chosen link belongs to the mutually generalized giant connected component (MGGCC) in each sub-network. Similarly, we define $\tilde{f}$ as the probability that a randomly selected link reaches the mutually giant connected component (MGCC) in each sub-network. The randomly selected node i in sub-network A belong to the MGGCC, if one of the following conditions is satisfied: (E_1) both node i and its dependency partner j in sub-network B reach the MGGCC, (E_2) its dependency partner j in sub-network B fails, causing the connectivity link of node i to disconnect from its neighbor nodes with probability $1 - \alpha_A$, but node i still leads to the MGGCC. The probabilities corresponding to E_1 and E_2 can be written out as

$$p(E_1) = p^2 \left[1 - (1 - \rho_A) G_1^A (1 - f_A)\right] \left[1 - (1 - \rho_B) G_0^B (1 - f_B)\right], \tag{B1}$$

$$p(E_2) = p\alpha_A \left[1 - (1 - \rho_A) G_1^A (1 - \alpha_A f_A)\right] \left\{1 - p\left[1 - (1 - \rho_B) G_0^B (1 - f_B)\right]\right\}. \tag{B2}$$

Where $p\left\{\rho_A + (1 - \rho_A) \sum \frac{p_A(k_A)k_A}{\langle k_A\rangle} \left[1 - (1 - f_A)^{k_A-1}\right]\right\} = p\left[1 - (1 - \rho_A) G_1^A (1 - f_A)\right]$ is the probability that one of the other $k_A - 1$ links of node i (the link that we first randomly chose is excluded) reaches the MGGCC of sub-network A. Here, p indicates that node i is not initially attacked. ρ_A is the probability that node i is reinforced in sub-network A. The probability

* Corresponding author (email: hongtaoyu_ndsc@163.com)

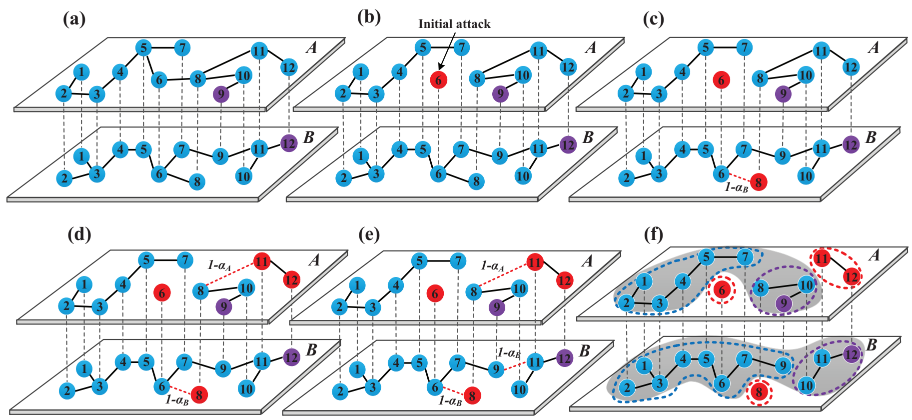

Figure A1 Illustration of dynamic process of cascading failures in interdependent networks with weak dependency links and reinforced nodes (WD-RN). (a) An example model with weak dependency links and reinforced nodes. Purple nodes are reinforced nodes. Here the black dotted lines and black solid lines represent the weak dependency links and connectivity links, respectively. (b) Node 6 of network A is initially attacked and fails. All connectivity links of node 6 are removed, triggering a cascading failure of the entire system. (c) Node 6 of the network B is impacted, and its connectivity links are deleted with a probability of $1-\alpha_B$ due to weak interdependence between networks A and B. Immediately, node 8 fails due to separation from the giant connected component of network B. (d) Node 8 of the network A is affected, and its connectivity links are removed with a probability of $1-\alpha_A$ due to weak interdependence. Consequently, small component(red dashed circle) containing nodes 11 and 12 fails by not containing reinforced nodes and disconnecting from the giant connected component(blue dashed circle) of network A. (e) Node 11 of the network B is impacted, and its connectivity links are dropped with a probability of $1-\alpha_B$ due to weak interdependence. However, small finite functional component(purple dashed circle) containing nodes 10 , 11, and 12 survives by containing reinforced node 12, even though disconnected from the giant connected component(blue dashed circle) of the network B. After this, there is no further failure and the process ends. (f) Finally, the system achieves a stable state. The blue circles constitute the MGCC. The MGGCC in the shaded gray areas consists of the MGCC and finite components supported by reinforced nodes.

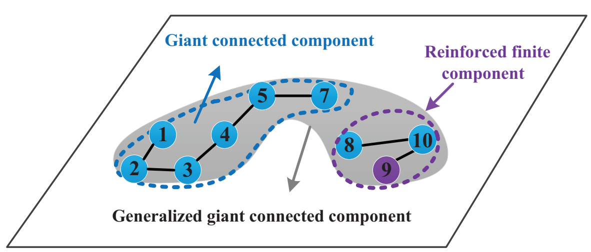

Figure A2 A schematic of a larger generalized giant connected component (GGCC) than the giant connected component (GCC) in a single-layer network. All the nodes of blue dashed circle constitute the GCC. The GCC is the largest connected component in a network. Finite components are the non-GCC in a network. Purple nodes are reinforced nodes. Reinforced finite components are defined as the finite components containing at least one reinforced node. The GGCC in grey shaded area is composed of the GCC and reinforced finite component.

Algorithm A1 Simulation of the cascading failures against random attack

Input: interdependent networks A and B with weak dependency links and reinforced nodes
Output: P_∞ and U_∞ in each network, respectively

```
for each node i in each network do
  for i = 1 to 1000000 do
    A fraction 1 − p of nodes are initially randomly attacked in network A and B, respectively;
    Remove the attacked nodes in networkA and B, respectively;
    int step;
    while The nodes in network A or B is still changing do
      step++;
      if step % = 2 then
        The nodes that do not belong to the MGGCC in network A will fail, and each connectivity
        link of its dependency partner in network B will be simultaneously removed with the failure
        probability 1 − α_B;
        Remove the nodes that do not belong to the MGGCC in network A;
      else
        The nodes that do not belong to the MGGCC in network B will fail, and each connectivity
        link of its dependency partner in network A will be simultaneously removed with the failure
        probability 1 − α_A;
        Remove the nodes that do not belong to the MGGCC in network B;
      end if
    end while
  end for
  Save the size of surviving nodes in the MGGCC (P_∞) and MGCC (U_∞) for each network, respec-
  tively;
end for
```

that node i belongs to the MGGCC is determined by either (i) being a reinforced node (ii) not being a reinforced node, but one of the other $k_A - 1$ links of node i (the link that we first randomly chose is excluded) leads to the MGGCC. Analogously, $p\left[1-(1-\rho_B)\,G_0^B\,(1-f_B)\right]$ is the probability that one of the k_B links of node j reaches the MGGCC of sub-network B. Owing to E_1 and E_2 being exclusive events, we obtain

$$f_A = P\,(E_1) + P\,(E_2)\,. \tag{B3}$$

Appendix B.2 Theoretical framework for general interdependent networks

Based on the probabilistic description in Appendix B.1, we can derive the following self-consistent equations about f_A and f_B according to the generating function:

$$f_A = p^2\left[1-(1-\rho_A)G_1^A\,(1-f_A)\right]\left[1-(1-\rho_B)\,G_0^B\,(1-f_B)\right] + p\alpha_A\left[1-(1-\rho_A)\,G_1^A\,(1-\alpha_A f_A)\right]\left\{1-p\left[1-(1-\rho_B)\,G_0^B\,(1-f_B)\right]\right\}, \tag{B4}$$

$$f_B = p^2\left[1-(1-\rho_B)G_1^B\,(1-f_B)\right]\left[1-(1-\rho_A)\,G_0^A\,(1-f_A)\right] + p\alpha_B\left[1-(1-\rho_B)\,G_1^B\,(1-\alpha_B f_B)\right]\left\{1-p\left[1-(1-\rho_A)\,G_0^A\,(1-f_A)\right]\right\}. \tag{B5}$$

Accordingly, the size of the MGGCC in sub-network $A(B)$ can be calculated as

$$P_\infty^A = p^2\left[1-(1-\rho_A)\,G_0^A\,(1-f_A)\right]\left[1-(1-\rho_B)\,G_0^B\,(1-f_B)\right] + p\left[1-(1-\rho_A)\,G_0^A\,(1-\alpha_A f_A)\right]\left\{1-p\left[1-(1-\rho_B)\,G_0^B\,(1-f_B)\right]\right\}, \tag{B6}$$

$$P_\infty^B = p^2\left[1-(1-\rho_B)\,G_0^B\,(1-f_B)\right]\left[1-(1-\rho_A)\,G_0^A\,(1-f_A)\right] + p\left[1-(1-\rho_B)\,G_0^B\,(1-\alpha_B f_B)\right]\left\{1-p\left[1-(1-\rho_A)\,G_0^A\,(1-f_A)\right]\right\}. \tag{B7}$$

Similarly, we denote $\tilde{f}_A$ $(\tilde{f}_B)$ as the probability that a randomly chosen link reaches the MGCC in sub-network $A(B)$, which can be written out as

$$\tilde{f}_A = p^2\left[1-G_1^A\left(1-\tilde{f}_A\right)\right]\left[1-(1-\rho_B)\,G_0^B\,(1-f_B)\right] + p\alpha_A\left[1-G_1^A\left(1-\alpha_A\tilde{f}_A\right)\right]\left\{1-p\left[1-(1-\rho_B)\,G_0^B\,(1-f_B)\right]\right\}, \tag{B8}$$

$$\tilde{f}_B = p^2\left[1-G_1^B\left(1-\tilde{f}_B\right)\right]\left[1-(1-\rho_A)\,G_0^A\,(1-f_A)\right] + p\alpha_B\left[1-G_1^B\left(1-\alpha_B\tilde{f}_B\right)\right]\left\{1-p\left[1-(1-\rho_A)\,G_0^A\,(1-f_A)\right]\right\}. \tag{B9}$$

Where $1-G_1^A\left(1-\tilde{f}_A\right)$ is the probability that one of the other $k_A - 1$ links of node i (the link that we first randomly chose is excluded) reaches the MGCC of sub-network A, and vice versa.

Consequently, the size of the MGCC in sub-network $A(B)$ can be computed as

$$U_\infty^A = p^2\left[1-G_0^A\left(1-\tilde{f}_A\right)\right]\left[1-(1-\rho_B)\,G_0^B\,(1-f_B)\right] + p\left[1-G_0^A\left(1-\alpha_A\tilde{f}_A\right)\right]\left\{1-p\left[1-(1-\rho_B)\,G_0^B\,(1-f_B)\right]\right\}, \tag{B10}$$

$$U_\infty^B = p^2\left[1-G_0^B\left(1-\tilde{f}_B\right)\right]\left[1-(1-\rho_A)\,G_0^A\,(1-f_A)\right] + p\left[1-G_0^B\left(1-\alpha_B\tilde{f}_B\right)\right]\left\{1-p\left[1-(1-\rho_A)\,G_0^A\,(1-f_A)\right]\right\}. \tag{B11}$$

As a result, these Eqs. (B4)- (B11) are proposed as general theoretical framework in our model. Note that, in Figure B1, Figure B2, and Figure B3, simulation results agree well with theoretical predictions, which indicates the validity of the general theoretical framework.

For simplicity, these (B1), (B2), (B5), and (B6) can be transformed into $f_A = F_1(p, f_B)$, $f_B = F_2(p, f_A)$, $\tilde{f}_A = R_1\left(p, \tilde{f}_A, f_B\right)$, and $\tilde{f}_B = R_2\left(p, \tilde{f}_B, f_A\right)$. Combining (B1), (B2), (B5), and (B6) together, we can obtain the numerical solutions of f_A, f_B, $\tilde{f}_A$, and $\tilde{f}_B$. Substituting the solutions back into (B3), (B4), (B7), and (B8), the theoretical numerical solutions of P_∞^A, P_∞^B, U_∞^A, and U_∞^B can be obtained.

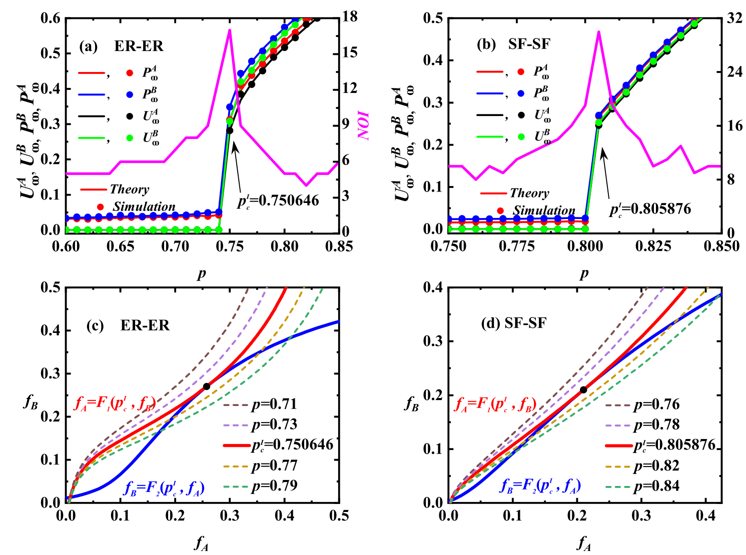

Figure B1 Demonstration of discontinuous phase transition in general ER-ER and SF-SF networks. (a) When $\alpha_A = 0.1$, $\alpha_B = 0.2$, and $\rho_A = \rho_B = 0.05$, P_∞^A, P_∞^A, P_∞^B, U_∞^A, U_∞^B, and NOI as a function of the probability p of preserving nodes in general ER-ER networks. Note that, P_∞^A, P_∞^B, U_∞^A, and U_∞^B undergo a discontinuous phase transition at the same p_c^I. (b) When $\rho_A = 0.02$, $\rho_B = 0.03$, and $\alpha_A = \alpha_B = 0.1$, P_∞^A, P_∞^B, U_∞^A, U_∞^B, and NOI as a function of the probability p of preserving nodes in general SF-SF networks. Note that, P_∞^A, P_∞^B, U_∞^A, and U_∞^B undergo a discontinuous phase transition at the same p_c^I. Numbers of cascade failure iterations (NOI) versus p in the simulation. Note that, NOI curves peak just right occur at discontinuous phase transition points p_c^I which is a method to identify the phase transition points p_c^I. (c) For general ER-ER networks illustrated in (a) with $p_c^I = 0.750646$, the curves of $f_A = F_1(p, f_B)$ and $f_B = F_2(p, f_A)$ touch each other tangentially at $f_A^I = 0.259749$ and $f_B^I = 0.272237$, satisfying (B12). (d) For general SF-SF networks illustrated in (b) with $p_c^I = 0.805876$, the curves of $f_A = F_1(p, f_B)$ and $f_B = F_2(p, f_A)$ touch each other tangentially at $f_A^I = 0.209455$ and $f_B^I = 0.209363$, satisfying (B12). Symbols represent simulation results and solid lines are the corresponding theoretical predictions. These simulation results are averaged 100 independent realizations. Other parameters are set to be $N = 10^6$, $\langle k_A\rangle = \langle k_B\rangle = 4$, $\lambda_A = \lambda_B = 2.6$, $k \in [2, 1000]$.

For the discontinuous (abrupt) phase transition, as depicted in Figure B1, the size of the MGGCC abruptly increases at $p = p_c^I$, and the function $f_A = F_1(p, f_B)$ and $f_B = F_2(p, f_A)$ at $p = p_c^I$ satisfy the condition

$$\frac{\partial F_1(p_c^I, f_B^I)}{\partial f_B^I}\cdot\frac{\partial F_2(p_c^I, f_A^I)}{\partial f_A^I} = 1, \tag{B12}$$

where the curves $f_A = F_1(p, f_B)$ and $f_B = F_2(p, f_A)$ touch each other tangentially at (f_A^I, f_B^I). Combining $f_A^I = F_1\left(p, f_B^I\right)$, $f_B^I = F_2\left(p, f_A^I\right)$, and (B12) together, the corresponding solutions of p_c^I, f_A^I, and f_B^I can be achieved. Note that P_∞^A, P_∞^B, U_∞^A, andU_∞^B have same discontinuous phase transition point at p_c^I.

Figure B2 and Figure B3 show that there is a critical shift point α_{A_c} ($\alpha_{A_c}^I$ or $\alpha_{A_c}^{II}$) of weak dependency parameter α_A for a given α_B. Above the critical threshold $\alpha_{A_c}^I$ ($\alpha_{A_c}^{II}$) , sub-network A (sub-network B) disintegrates in the form of a continuous phase transition. Conversely, sub-network A (sub-network B) suffers from a discontinuous phase transition. One interesting finding in ER-ER networks is that Figure B2(b) shows a phenomenon of hybrid phase transition. Due to an iterative process of cascading failures, the MGCC (U_∞^A) of the sub-network A discontinuously decreases to a relatively small value at p_c^I and then continuously decreases to zero at $p_c^{II}\mid_{U_\infty^A}$. Another unexpected finding in Figure B2(b), Figure B2(c), Figure B3(b), and Figure B3(c) is that with increasing α_A, the continuous phase transition in sub-network A is earlier than that in sub-network B. Based on the above analysis, when $0 < \alpha_A \leqslant \alpha_{A_c}^I$, the entire system presents a discontinuous phase transition. When $\alpha_{A_c}^I \leqslant \alpha_A \leqslant \alpha_{A_c}^{II}$, it exhibits mixed phase transition characteristics, i.e., a hybrid phase transition for sub-network A and a discontinuous phase transition for sub-network B. When $\alpha_A \geqslant \alpha_{A_c}^{II}$, the whole system presents a continuous phase transition.

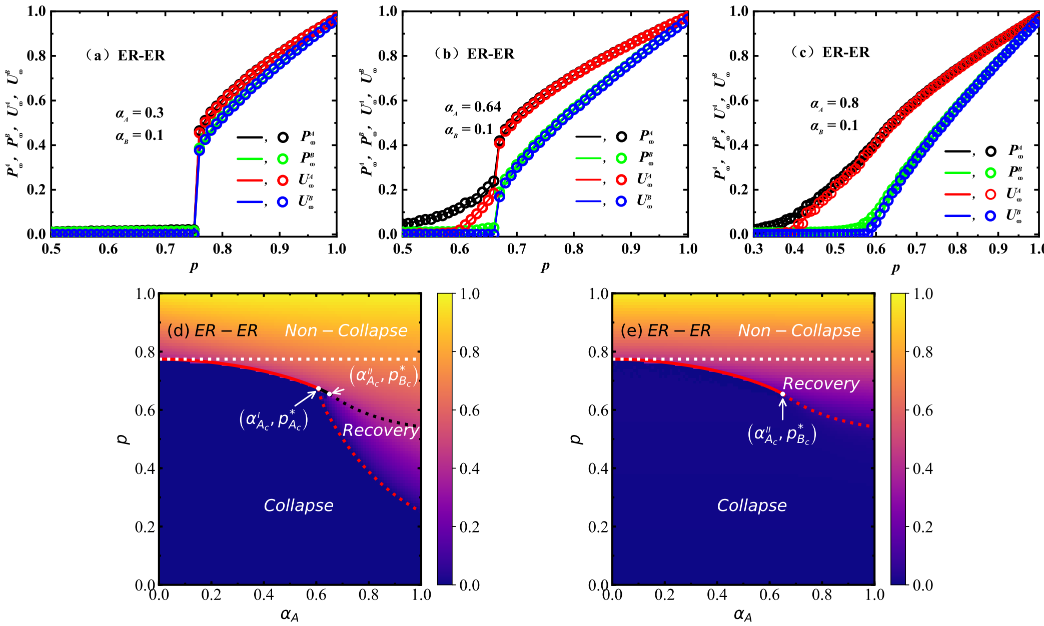

Figure B2 Demonstration of discontinuous, hybrid, continuous phase transition, and shift point of phase transition types in general ER-ER networks. (a)-(c): For different $\alpha_A = 0.3$, $\alpha_A = 0.64$, and $\alpha_A = 0.8$, P_∞^A, P_∞^B, U_∞^A, and U_∞^B as a function of the probability p of preserving nodes in general ER-ER networks. (a) P_∞^A, P_∞^B, U_∞^A, and U_∞^B undergo a discontinuous phase transition at the same p_c^I. (b) U_∞^A undergoes a hybrid phase transition, while P_∞^A, P_∞^B, and U_∞^B undergo a discontinuous phase transition at the same p_c^I. (c) U_∞^A and U_∞^B undergo a continuous phase transition at $p_c^{II} \mid_{U_\infty^A}$ and $p_c^{II} \mid_{U_\infty^B}$, while P_∞^A and P_∞^B are continuous and free of phase transition. (d) In sub-network A, color represents the theoretical results of P_∞^A $\left(\alpha_A < \alpha_{A_c}^I\right)$ and U_∞^A $\left(\alpha_A > \alpha_{A_c}^I\right)$ in plane (α_A, p). (e) In sub-network B, color represents the theoretical results of P_∞^B $\left(\alpha_A < \alpha_{A_c}^{II}\right)$ and U_∞^B $\left(\alpha_A > \alpha_{A_c}^{II}\right)$ in plane (α_A, p). The red solid lines in both (d) and (e) are the discontinuous percolation transition thresholds p_c^I, which are obtained by solving (B12). The red dashed line in (d) are the continuous percolation transition threshold $p_c^{II} \mid_{U_\infty^A}$, which are obtained by solving (B15). The black dashed line in (d) and the red dashed line in (e) are the continuous percolation transition threshold $p_c^{II} \mid_{U_\infty^B}$, which are obtained by solving (B16). Symbols represent simulation results and solid lines behind the symbols are the corresponding theoretical predictions. These simulation results are averaged 100 independent realizations. Other parameters are set to be $N = 10^6$, $\alpha_B = 0.1$, $\rho_A = \rho_B = 0.02$, and $\langle k_A \rangle = \langle k_B \rangle = 4$.

For the continuous phase transition, as shown in Figure B2(b), Figure B2(c), Figure B3(b), and Figure B3(c), one unanticipated finding is that the size of the MGCC $U_\infty^A (U_\infty^B)$ increases continuously at the transition point $p_c^{II} \mid_{U_\infty^A}$ $(p_c^{II} \mid_{U_\infty^B})$, yet the MGGCC P_∞^A (P_∞^B) is free of phase transition. Above the threshold p_c^{II}, with the increase of p, the size of the MGCC continuously increases from 0. Conversely, below the threshold p_c^{II}, the MGCC is absent. Thus, when $p \to p_c^{II} \mid_{U_\infty^A}$, we can analytically derive $\tilde{f}_A \to 0$. We further have a Taylor expansion of (B8) at $\tilde{f}_A \to 0$:

$$\tilde{f}_A = R_1^{'}\left(p_c^{II}, 0, f_B\right)\tilde{f}_A + \frac{1}{2!}R_1^{''}\left(p_c^{II}, 0, f_B\right)\tilde{f}_A^2 + o\left(\tilde{f}_A^3\right). \tag{B13}$$

After the simplification, we have

$$R_1^{'}\left(p_c^{II}, 0, f_B\right) + \frac{1}{2!}R_1^{''}\left(p_c^{II}, 0, f_B\right)\tilde{f}_A + o\left(\tilde{f}_A^2\right) = 1, \tag{B14}$$

and the nontrivial solution of (B8) appears when $R_1^{'}\left(p_c^{II}, 0, f_B\right) = 1$.

If sub-network A has continuous phase transition at $p = p_c^{II}$ for U_∞^A, $p_c^{II} \mid_{U_\infty^A}$ satisfies the condition

$$R_1^{'}\left(p_c^{II} \mid_{U_\infty^A}, 0, f_B\right) = 1, \quad \alpha_A > \alpha_{A_c}^I. \tag{B15}$$

Combining (B4), (B5), (B9), and (B15) together, $p_c^{II} \mid_{U_\infty^A}$ can be obtained numerically.

If sub-network B has continuous phase transition at $p = p_c^{II}$ for U_∞^B, $p_c^{II} \mid_{U_\infty^B}$ satisfies the condition

$$R_2^{'}\left(p_c^{II} \mid_{U_\infty^B}, 0, f_A\right) = 1, \quad \alpha_A > \alpha_{A_c}^{II}. \tag{B16}$$

Combining (B4), (B5), (B8), and (B16) together, $p_c^{II} \mid_{U_\infty^B}$ can be obtained numerically.

As shown in Figure B2(d), Figure B2(e), Figure B3(d), and Figure B3(e), By letting $p_c^I = p_c^{II} \mid_{U_\infty^A} = p_{A_c}^*$, we can obtain the shift point $\alpha_{A_c}^I$, at which there is a change from a discontinuous phase transition to a continuous phase transition of sub-network A. Furthermore, $\alpha_{A_c}^I$ is also the boundary between the discontinuous phase transition and the hybrid phase transition of the

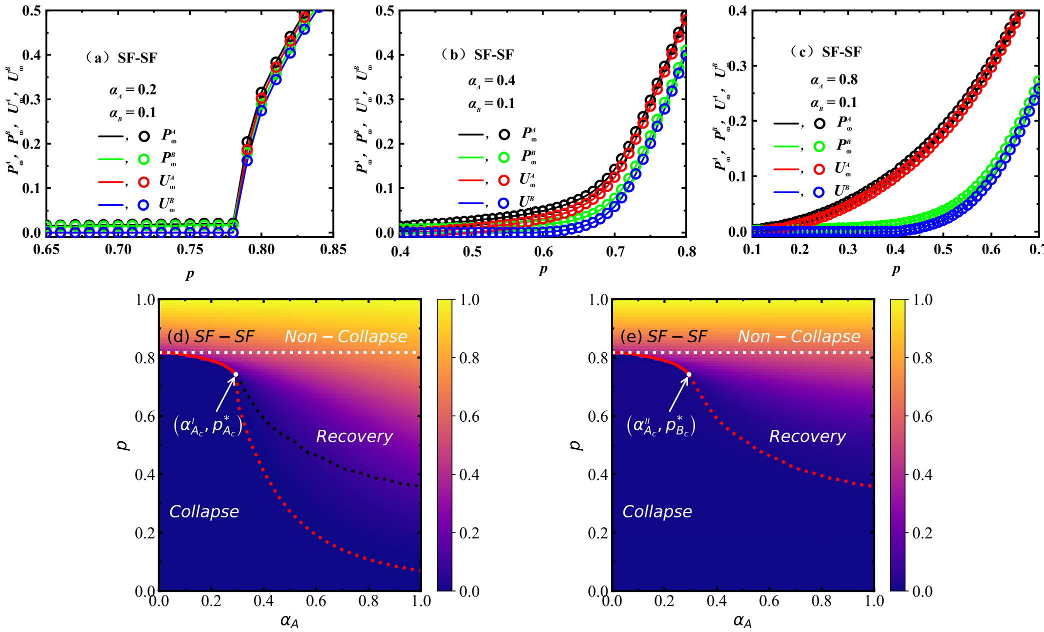

Figure B3 Demonstration of discontinuous, continuous phase transition, and shift point of phase transition types in general SF-SF networks. (a)-(c): For different $\alpha_A = 0.2$, $\alpha_A = 0.4$, and $\alpha_A = 0.8$, P_∞^A, P_∞^B, U_∞^A, and U_∞^B as a function of the probability p of preserving nodes in general SF-SF networks. (a) P_∞^A, P_∞^B, U_∞^A, and U_∞^B undergo a discontinuous phase transition at the same p_c^I. In (b) and (c), U_∞^A and U_∞^B undergo a continuous phase transition at $p_c^{II}\mid_{U_\infty^A}$ and $p_c^{II}\mid_{U_\infty^B}$, while P_∞^A and P_∞^B are continuous and free of phase transition. (d) In sub-network A, color represents the theoretical results of $P_\infty^A\left(\alpha_A < \alpha_{A_c}^I\right)$ and $U_\infty^A\left(\alpha_A > \alpha_{A_c}^I\right)$ in plane (α_A, p). (e) In sub-network B, color represents the theoretical results of $P_\infty^B\left(\alpha_A < \alpha_{A_c}^{II}\right)$ and $U_\infty^B\left(\alpha_A > \alpha_{A_c}^{II}\right)$ in plane (α_A, p). The red solid lines in both (d) and (e) are the discontinuous percolation transition thresholds p_c^I, which are obtained by solving (B12). The red dashed line in (d) are the continuous percolation transition threshold $p_c^{II}\mid_{U_\infty^A}$, which are obtained by solving (B15). The black dashed line in (d) and the red dashed line in (e) are the continuous percolation transition threshold $p_c^{II}\mid_{U_\infty^B}$, which are obtained by solving (B16). Symbols represent simulation results and solid lines behind the symbols are the corresponding theoretical predictions. These simulation results are averaged 100 independent realizations. Other parameters are set to be $N = 10^6$, $\alpha_B = 0.1$, $\rho_A = \rho_B = 0.02$, and $\langle k_A\rangle = \langle k_B\rangle = 4$, $\lambda_A = \lambda_B = 2.6$, $k \in [2, 1000]$.

whole system. Using the same method, we can get the shift point $\alpha_{A_c}^{II}$ by letting $p_c^I = p_c^{II}\mid_{U_\infty^B} = p_{B_c}^*$, at which there is a change from a discontinuous phase transition to a continuous phase transition of sub-network B. Furthermore, $\alpha_{A_c}^{II}$ is also the boundary between the hybrid phase transition and the continuous phase transition of the whole system. Note that, when $p_{A_c}^* \neq p_{B_c}^*$ (i.e., $\alpha_{A_c}^I \neq \alpha_{A_c}^{II}$), the system will exhibit a hybrid phase transition behavior, as shown in Figure B2(b). Conversely, when $p_{A_c}^* = p_{B_c}^*$ (i.e., $\alpha_{A_c}^I = \alpha_{A_c}^{II}$), the system has no hybrid phase transition behavior, as illustrated in Figure B3.

Appendix B.3 Results and discussion for general interdependent networks

Numerical simulations are constructed in Erdős-Rényi (ER) and scale-free (SF) networks, which are general methods used to predict the robustness of real-life networks. For ER-ER networks, the degree distribution satisfies $p(k) = \frac{\langle k\rangle^k e^{-\langle k\rangle}}{k!}$, where $\langle k\rangle$ denotes the average degree. For SF-SF networks, the degree distribution satisfies $p(k) \sim k^{-\lambda}$, where $\langle k\rangle$ denotes the average degree, $k \in [2, 1000]$, and λ denotes the degree exponent. These simulation results are averaged over 100 independent realizations, where node size of each sub-network is $N = 10^6$. The simulation results (symbols) agree well with theoretical predictions (solid lines) in Figure B1, Figure B2, and Figure B3.

In Figure B1(a), when $\alpha_A < \alpha_B$, there are $P_\infty^A < P_\infty^B <$ and $U_\infty^A < U_\infty^B$. In Figure B2 and Figure B3, when $\alpha_A > \alpha_B$, there are $P_\infty^A > P_\infty^B$ and $U_\infty^A > U_\infty^B$, and thus the robustness of sub-network with large weak dependency parameter is higher than that of sub-network with small weak dependency parameter. For sub-network A(sub-network B), when the fraction of reinforced nodes $\rho_A > 0$ ($\rho_B > 0$), there is $P_\infty^A > U_\infty^A$ ($P_\infty^B > U_\infty^B$), indicating that equipping reinforced nodes can enhance the robustness of the system.

As shown in Figure B2(a), Figure B2(b), and Figure B2(c), for a given weak dependency parameter $\alpha_B = 0.1$, with the increasing of α_A, the system exhibits different type of phase transitions. For $\alpha_A = 0.3$, both sub-network A and sub-network B percolate discontinuously at the same point p_c^I. For $\alpha_A = 0.64$, sub-network A exhibits a rich phase transition behavior: P_∞^A undergoes a discontinuous phase transition at p_c^I, and U_∞^A discontinuously decreases to a relatively small value at p_c^I and then continuously decreases to zero at $p_c^{II}\mid_{U_\infty^A}$, while sub-network B exhibits a discontinuous phase transition at p_c^I. For $\alpha_A = 0.8$, both sub-network A and sub-network B percolate continuously at different phase transition point: U_∞^A and U_∞^B undergo a continuous phase transition at $p_c^{II}\mid_{U_\infty^A}$ and $p_c^{II}\mid_{U_\infty^B}$, respectively, while P_∞^A and P_∞^B are continuous and free of phase transition. Surprisingly, in Figure B2(c), for $\alpha_A = 0.8 > \alpha_B = 0.1$, we find $p_c^{II}\mid_{U_\infty^A} < p_c^{II}\mid_{U_\infty^B}$.

Next, in general ER-ER networks, for sub-network A, the sizes of $P_\infty^A\left(\alpha_A < \alpha_{A_c}^I\right)$ and $U_\infty^A\left(\alpha_A > \alpha_{A_c}^I\right)$ in plane (α_A, p) is studied systematically in Figure B2(d). For sub-network B, the sizes of $P_\infty^B\left(\alpha_A < \alpha_{A_c}^{II}\right)$ and $U_\infty^B\left(\alpha_A > \alpha_{A_c}^{II}\right)$ in plane (α_A, p) in

Figure B2(e). $P_\infty^A\left(\alpha_A<\alpha_{A_c}^I\right)$ and $P_\infty^B\left(\alpha_A<\alpha_{A_c}^{II}\right)$ increase as α_A increases in plane (α_A,p), and increase as p increases in plane (α_A,p). $U_\infty^A\left(\alpha_A>\alpha_{A_c}^I\right)$ and $U_\infty^B\left(\alpha_A>\alpha_{A_c}^{II}\right)$ increase as α_A increases in plane (α_A,p), and increase as p increases in plane (α_A,p). In Figure B2(e), the plane are divided into functional $(P_\infty^B>0,U_\infty^B>0)$ and non-functional region$(P_\infty^B=0,U_\infty^B=0)$ region by the red line. Here the white dashed line is the discontinuous phase transition threshold when there are strong dependency links $(\alpha_A=0)$, which is also the baseline of the phase transition compared to the weak dependency links $(\alpha_A>0)$. Further, the functional region is divided into non-collapse and recovery regions by the white dashed line. This division is to reflect the difference between strong dependency links and weak dependency links, i.e., as the value of the weak dependency parameter α_A increases from zero, the middle region changes from the original non-functional region $(P_\infty^B=0,U_\infty^B=0)$ to the functional region$(P_\infty^B>0,U_\infty^B>0)$, which is equivalent to the recovery region according to the network state. As a result, the plane is clearly divided into non-collapse, recovery, and collapse regions by the red line and the white dashed line.

In sub-network A (Figure B2(d)), with the decrease of p, for $\alpha_A\leqslant\alpha_{A_c}^I$, P_∞^A is greater than zero when $p>p_c^I$, and decreases discontinuously to zero at $p=p_c^I$; for $\alpha_A>\alpha_{A_c}^I$, U_∞^A is greater than zero when $p>p_c^{II}\mid_{U_\infty^A}$, and decreases continuously to zero at $p=p_c^{II}\mid_{U_\infty^A}$; for $\alpha_{A_c}^I\leqslant\alpha_A\leqslant\alpha_{A_c}^{II}$, U_∞^A is larger than zero when $p>p_c^{II}\mid_{U_\infty^A}$, and first discontinuously decreases to a relatively small value at p_c^I and then continuously decreases to zero at $p_c^{II}\mid_{U_\infty^A}$. In sub-network B (Figure B2(e)), with the decrease of p, for $\alpha_A\leqslant\alpha_{A_c}^{II}$, P_∞^B is greater than zero when $p>p_c^I$, and decreases discontinuously to zero at $p=p_c^I$; for $\alpha_A>\alpha_{A_c}^{II}$, U_∞^B is greater than zero when $p>p_c^{II}\mid_{U_\infty^B}$, and decreases continuously to zero at $p=p_c^{II}\mid_{U_\infty^B}$.

As shown in Figure B3, similar theoretical and simulation results are discussed in the general SF-SF networks. Different from the results shown in Figure B2, U_∞^A of the general SF-SF networks has no hybrid phase transition behavior (i.e., $\alpha_{A_c}^I=\alpha_{A_c}^{II}$). Note that, compared with the general ER-ER networks, the size of U_∞^A(or U_∞^B) in the general SF-SF networks changes more smoothly and gently at the continuous phase transition point $p=p_c^{II}\mid_{U_\infty^A}$ (or $p=p_c^{II}\mid_{U_\infty^B}$) , which makes the plane (α_A,p) not so clearly divided by the red dotted line boundary.

Appendix C Solving interdependent networks with symmetry

Appendix C.1 Theoretical framework for interdependent networks with symmetry

To better capture the percolation phase transition properties of the proposed model, here we introduce simple symmetric interdependent networks with $p_A(k_A)=p_B(k_B)=p(k)$, $\langle k_A\rangle=\langle k_B\rangle=\langle k\rangle$, $\rho_A=\rho_B=\rho$, and $\alpha_A=\alpha_B=\alpha$. Thus, we have $f_A=f_B\equiv f$, $P_\infty^A=P_\infty^B\equiv P_\infty$, $\tilde f_A=\tilde f_B\equiv\tilde f$, and $U_\infty^A=U_\infty^B\equiv U_\infty$. These (B4) - (B11) can be simplified as

$$f=u(f)\,p^2+v(f)\,p\equiv F(p,f)\,, \tag{C1}$$

$$P_\infty=p^2\left[1-(1-\rho)\,G_0(1-f)\right]\left[1-(1-\rho)\,G_0(1-f)\right]\ +p\left[1-(1-\rho)\,G_0(1-\alpha f)\right]\left\{1-p\left[1-(1-\rho)\,G_0(1-f)\right]\right\}, \tag{C2}$$

$$\tilde f=p^2\left[1-G_1\left(1-\tilde f\right)\right]\left[1-(1-\rho)\,G_0(1-f)\right]+p\alpha\left[1-G_1\left(1-\alpha\tilde f\right)\right]\left\{1-p\left[1-(1-\rho)\,G_0(1-f)\right]\right\}\equiv R\left(p,\tilde f,f\right), \tag{C3}$$

$$U_\infty=p^2\left[1-G_0\left(1-\tilde f\right)\right]\left[1-(1-\rho)\,G_0(1-f)\right]\ +p\left[1-G_0\left(1-\alpha\tilde f\right)\right]\left\{1-p\left[1-(1-\rho)\,G_0(1-f)\right]\right\}, \tag{C4}$$

where $u(f)=\{[1-(1-\rho)\,G_1\ (1-f)]-\alpha\,[1-(1-\rho)\,G_1\ (1-\alpha f)]\}\,[1-(1-\rho)\,G_0\ (1-f)]$, $v(f)=\alpha\,[1-(1-\rho)\,G_1\ (1-\alpha f)]$, and $H(f)=F(p,f)-f$.

As a result, these (C1)-(C4) are proposed as the theoretical framework for interdependent networks with symmetry. Note that, in Figure C1 and Figure C2, simulation results agree well with theoretical predictions, which further indicates the validity of the theoretical framework.

Figure C1 illustrates that there is a triple point (ρ_c^*,p_c^*) or (α_c^*,p_c^*). At the triple point, the system satisfies the discontinuous and continuous phase transition, simultaneously. Below the critical threshold $\rho<\rho_c^*$(or $\alpha<\alpha_c^*$), the system undergoes a discontinuous phase transition. Above the threshold $\rho>\rho_c^*$(or $\alpha>\alpha_c^*$), the system suffers a continuous phase transition. Figure C2 further shows that the MGGCC (P_∞) and MGCC (U_∞) have the same phase transition points for different ρ ($\rho\leqslant\rho_c^*$) in each sub-network.

If the system has a discontinuous phase transition at $p=p_c^I$ when $\rho<\rho_c^*$, (B12) is simplified to $\frac{\partial F\left(p_c^I,f^I\right)}{\partial f^I}=1$, namely

$$u'\left(f^I\right)\left(p_c^I\right)^2+v'\left(f^I\right)p_c^I-1=0. \tag{C5}$$

One unanticipated finding in Figure C3 is that, when $p=p_c^I$, the curve $H(f)$ is just tangent to the f-axis, i.e., $\frac{\partial F\left(p_c^I,f^I\right)}{\partial f^I}-1=0$, which further verifies the correctness of our theoretical analysis. Thus, we can obtain the discontinuous transition point

$$p_c^I\left(f^I\right)=\frac{-v'\left(f^I\right)+\sqrt{\Delta}}{2u'\left(f^I\right)},\quad \Delta=\left[v'\left(f^I\right)\right]^2+4u'\left(f^I\right)>0,\quad \rho<\rho_c^*, \tag{C6}$$

where f^I can be numerically solved by (C1) and (C5).

If the system has a continuous phase transition for U_∞ at phase transition point $p_c^{II}\mid_{U_\infty}$ when $\rho>\rho_c^*$, we have $\tilde f=0$. Thus, (B15) and (B16) are equivalent, reduced to

$$R'\left(p_c^{II}\mid_{U_\infty},0,f\right)=1,\quad \rho>\rho_c^*. \tag{C7}$$

Combining (C1) and (C7) together, $p_c^{II}\mid_{U_\infty^A}$ can be obtained numerically. In particular, when $\rho=0$, there is no reinforced nodes in the system, for ER-ER interdependent networks, this yields

$$p_c^{II}\mid_{U_\infty}=\frac{1}{\alpha^2\langle k\rangle},\quad \rho=0,\quad \alpha>\alpha_{\max}^*, \tag{C8}$$

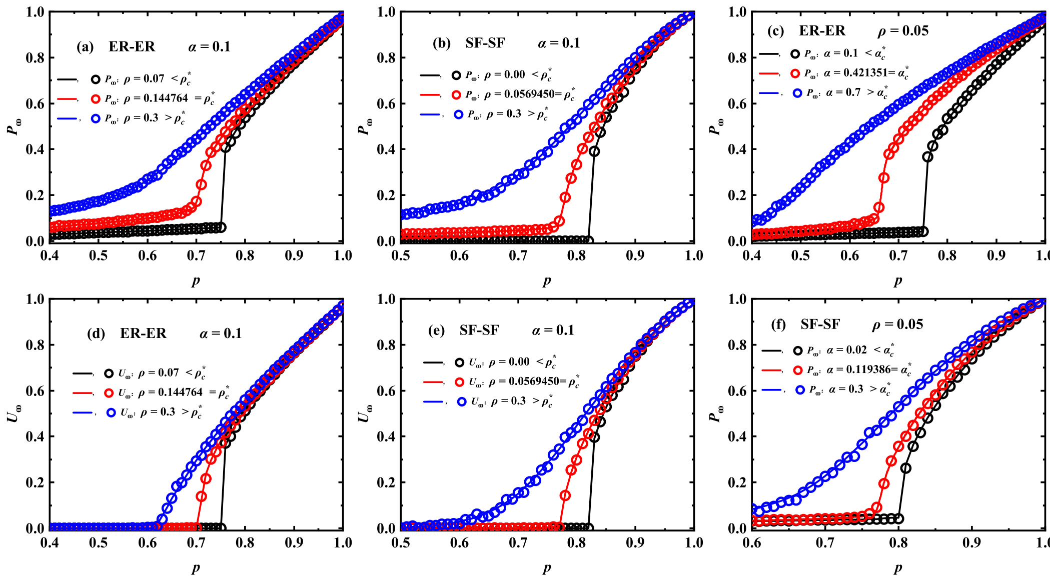

Figure C1 The sizes of P_∞ and U_∞ as a function of the probability p of preserving nodes in ER-ER and SF-SF networks. In (a) and (d), fixing $\alpha = 0.1$, comparison of simulation and theoretical results for different ρ in ER-ER networks; In (b) and (e), fixing $\alpha = 0.1$, comparison of simulation and theoretical results for different ρ in SF-SF networks; In (c) and (f), fixing $\rho = 0.05$, comparison of simulation and theoretical results of different α in ER-ER and SF-SF networks. Symbols represent simulation results and solid lines are the corresponding theoretical predictions. Other parameters are set to be $N = 10^6$, $\langle k \rangle = 4$, $\lambda = 2.6$, and $k \in [2, 1000]$.

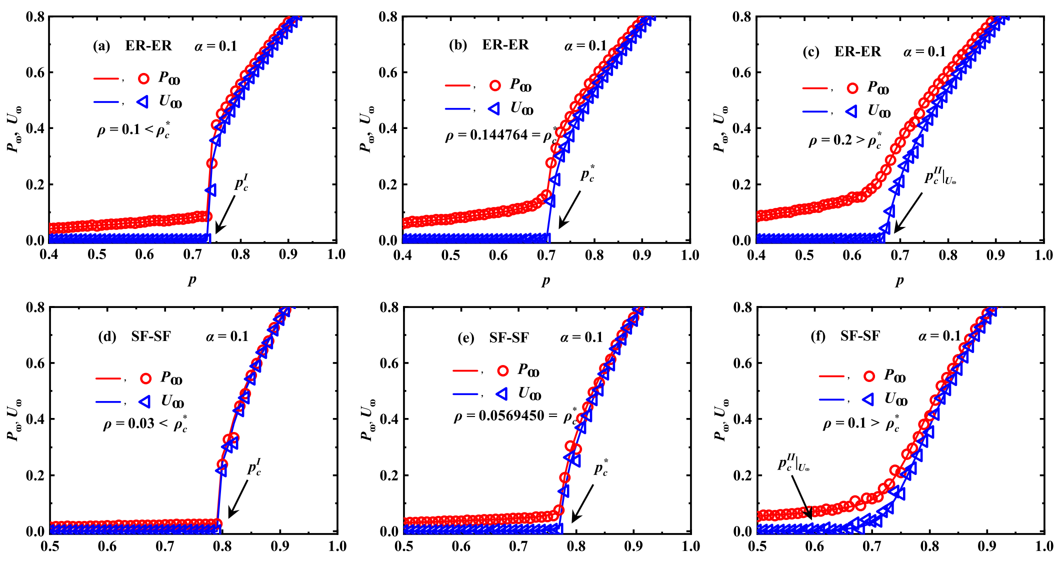

Figure C2 The sizes of P_∞ and U_∞ as a function of the probability p of preserving nodes for different ρ in ER-ER and SF-SF networks. In (a) and (d), when $\rho <= \rho_c^*$, both P_∞ and U_∞ undergo a discontinuous phase transition at the same p_c^I; In (b) and (e), when $\rho = \rho_c^*$, the system has both continuous and discontinuous phase transition properties at the same p_c^*; In (c) and (f), when $\rho >= \rho_c^*$, U_∞ undergoes a continuous phase transition at $p_c^{II} \mid_{U_\infty}$, and P_∞ is continuous and free of phase transition. Symbols represent simulation results and solid lines are the corresponding theoretical predictions. Other parameters are set to be $N = 10^6$, $\alpha = 0.1$, $\langle k \rangle = 4$, $\lambda = 2.6$, and $k \in [2, 1000]$.

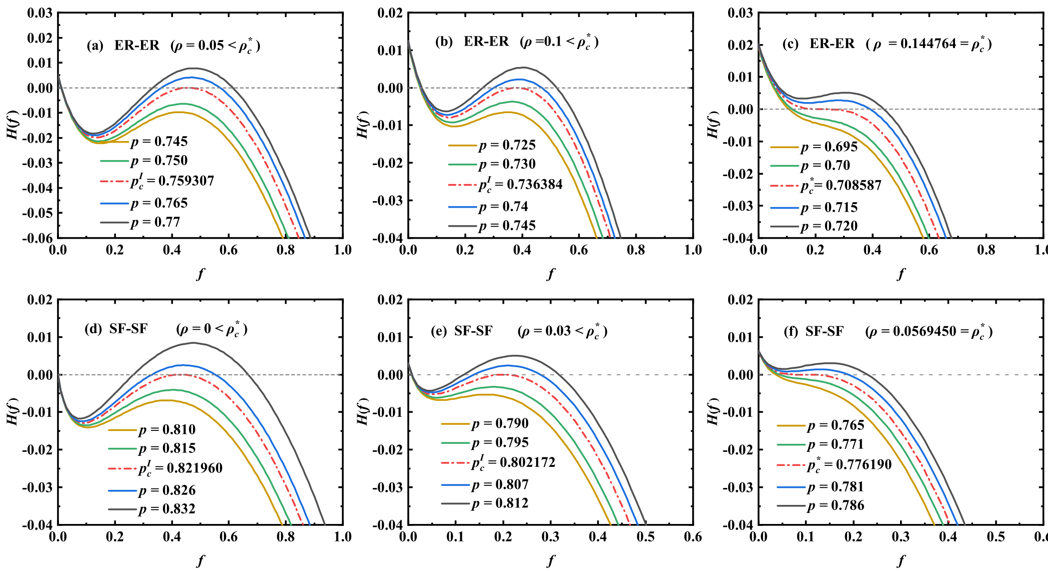

Figure C3 Graphical solutions of (C1) for different p in ER-ER and SF-SF interdependent networks, where $H(f) = F(p, f) - f$. In (a) and (b), with the increase of p, for $\rho < \rho_c^*$, the curve $H(f)$ is firstly tangent to the f-axis at the point p_c^I. In (c) and (f), with the increase of p, for $\rho = \rho_c^*$, the curve $H(f)$ is firstly tangent to the f-axis at the point p_c^*. For a discontinuous percolation transition threshold p_c^I(i.e., $\rho < \rho_c^*$), there are 2 extreme points and the maximum extreme point is tangent to f-axis, and for a continuous percolation transition threshold p_c^* (i.e.,$\rho = \rho_c^*$), the two extreme points just right coincide and are tangent to the f-axis. One interesting finding is that ρ_c^*can be used as the boundary value to distinguish between discontinuous percolation transition and continuous percolation transition. Note that, when $\rho > \rho_c^*$, there is no solution of (C1). Other parameters are set to be $\alpha = 0.1$, $\langle k \rangle = 4$, $\lambda = 2.6$, and $k \in [2, 1000]$.

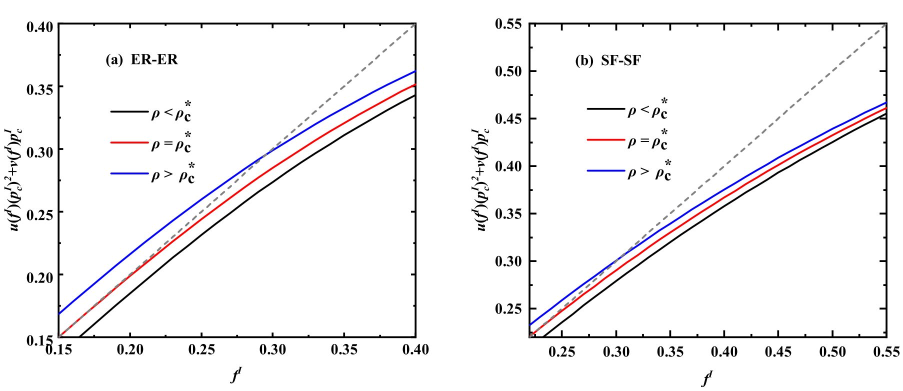

Figure C4 Graphical solutions of (C6) and (C9) for different ρ in and SF-SF interdependent networks. (a) ER-ER networks: $\alpha = 0.1$ and $\langle k \rangle = 4$; (b) SF-SF networks: $\alpha = 0.1$, $\langle k \rangle = 4$, $\lambda = 2.6$, and $k \in [2, 1000]$.

where $\langle k \rangle$ is the average degree in each network.

Further, plugging p_c^I back into (C1), we obtain

$$f^I = u\left(f^I\right)\left(p_c^I\right)^2 + v\left(f^I\right)p_c^I \equiv F\left(p_c^I, f^I\right). \tag{C9}$$

One interesting finding in Figure C4 is that when $\rho < \rho_c^*$, the curve $u\left(f^I\right)\left(p_c^I\right)^2 + v\left(f^I\right)p_c^I$ is separated from the dashed line; when $\rho = \rho_c^*$, the curve is tangent to the dashed line; when $\rho > \rho_c^*$, the curve is intersected by the dashed line. Obviously, the critical threshold $\rho = \rho_c^*$ satisfies the following condition that the derivative of both ends of (C9) with respect to f^I, namely

$$u'\left(f^I\right)\left(p_c^I\right)^2 + v'\left(f^I\right)p_c^I + \left[2u\left(f^I\right) + v\left(f^I\right)\right]\frac{dp_c^I}{df^I} = 1. \tag{C10}$$

Plugging (C5) back into (C10), this yields

$$\frac{dp_c^I}{df^I}\mid_{\rho=\rho_c^*(or\alpha=\alpha_c^*),p_c^I=p_c^{II}=p_c^*} = 0. \tag{C11}$$

Combining (C1), (C6), and (C11), fixing the parameter α, we can obtain numerically the triple point (ρ_c^*, p_c^*). More interestingly, fixing the parameter ρ, we will derive an equivalent triple point (α_c^*, p_c^*). Note that, ρ_c^* (α_c^*) is the critical threshold for discontinuous and continuous phase transitions in each sub-network, so ρ_c^* is also the minimum fraction of reinforced nodes needed to prevent a abrupt and catastrophic collapse of the interdependent system. Accordingly, fixed the parameter ρ, α_c^* is set to the minimum fraction of weak interdependent strength to prevent catastrophic collapse of the system.

Appendix C.2 Results and discussion for interdependent networks with symmetry

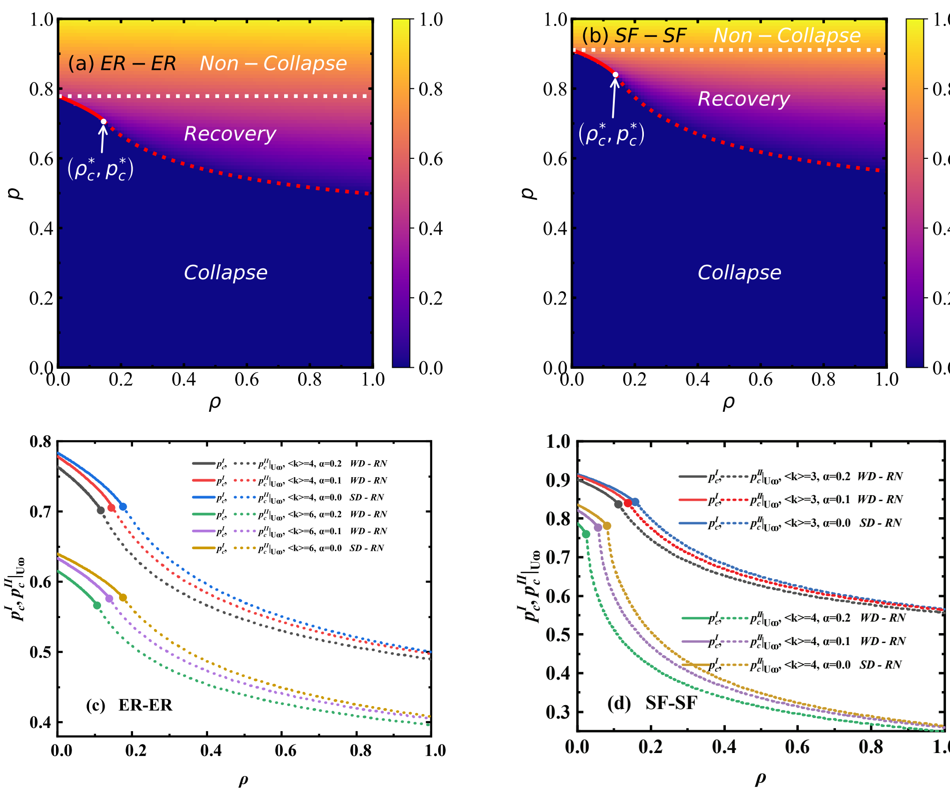

Figure C5 Phase diagrams in plane (ρ, p). (a) ER-ER networks with symmetry: $\langle k_A \rangle = \langle k_B \rangle = 6$, $\alpha_A = \alpha_B = 0.2$; (b) SF-SF networks with symmetry: $\langle k_A \rangle = \langle k_B \rangle = 3$, $\alpha_A = \alpha_B = 0.2$, $\lambda_A = \lambda_B = 2.6$, $k \in [2, 1000]$. Color in both (a) and (b) represents the theoretical values of P_∞ $(\rho < \rho_c^*)$ and U_∞ $(\rho > \rho_c^*)$ in plane (ρ, p). The red solid lines in both (a) and (b) are the discontinuous percolation transition thresholds p_c^I, which are obtained by solving (C6). The red dashed lines in both (a) and (b) are the continuous percolation transition threshold $p_c^{II}\mid_{U_\infty^A}$, which are obtained by solving (C7). (c) ER-ER networks with symmetry: p_c^I and $p_c^{II}\mid_{U_\infty}$ as a function of ρ for different $\langle k \rangle$ and α; (d) SF-SF networks with symmetry: p_c^I and $p_c^{II}\mid_{U_\infty}$ as a function of ρ for different $\langle k \rangle$ and α.

Numerical simulations are constructed in Erdős-Rényi (ER) and scale-free (SF) networks, which are general methods used to predict the robustness of real-life networks. For ER-ER networks, the degree distribution satisfies $p(k) = \frac{\langle k \rangle^k e^{-\langle k \rangle}}{k!}$, where $\langle k \rangle$ denotes the average degree. For SF-SF networks, the degree distribution satisfies $p(k) \sim k^{-\lambda}$, where $\langle k \rangle$ denotes the average degree, $k \in [2, 1000]$, and λ denotes the degree exponent. These simulation results are averaged over 100 independent realizations, where node size of each sub-network is $N = 10^6$. The simulation results (symbols) agree well with theoretical predictions (solid lines) in Figure C1 and Figure C2.

As shown in Figure C1(a), Figure C1(b), Figure C1(d), and Figure C1(e), for a given weak dependency parameter $\alpha = 0.1$, the sizes of mutually generalized giant connected component (MGGCC) and mutually giant connected component (MGCC) increase with the increase of the fraction p of preserved nodes. When p is fixed, P_∞ and U_∞ increase as the increase of ρ and the system shows different type of phase transitions in ER-ER networks and SF-SF networks. What's more, in Figure C2(a) and Figure C2(d), when $\rho <= \rho_c^*$, both P_∞ and U_∞ undergo a discontinuous phase transition at the same p_c^I; in Figure C2(b) and (e), when $\rho = \rho_c^*$, the system has both continuous and discontinuous phase transition properties at the same p_c^*; in Figure C2(c) and Figure C2(f), when $\rho >= \rho_c^*$, U_∞ undergoes a continuous phase transition at $p_c^{II}\mid_{U_\infty}$, and P_∞ is continuous and free of phase transition. Importantly, the percolation transition threshold (i.e., p_c^I and $p_c^{II}\mid_{U_\infty}$) decreases with the increase of ρ. In other words, increasing the fraction ρ of reinforced nodes can significantly enhance the robustness of interdependent networks. Note that , for a given $\rho > 0$, there is $P_\infty >= U_\infty$ in Figure C2, which further proves from theory and simulation that the reinforced nodes can support the function of small finite component where it is located, even if the small finite component is disconnected from the MGCC, indicating that equipped reinforced nodes can improve the system robustness.

As depicted in Figure C1(c) and Figure C1(f), for a given fraction $\rho = 0.05$ of reinforced nodes, when p is fixed, P_∞ increases as the increase of α and the system shows different type of phase transitions in ER-ER networks and SF-SF networks. Analogously, the percolation transition threshold (i.e., p_c^I and $p_c^{II}\mid_{U_\infty}$) decreases with the increase of α. Here, α_c^* can be used as the boundary value to distinguish between discontinuous percolation transition and continuous percolation transition. In other words, increasing the weak dependency parameter α can significantly enhance the robustness of interdependent networks.

Next, phase diagrams in plane (ρ, p) is studied systematically in Figure C5. As shown in Figure C5(a) and Figure C5(b), P_∞ $(\rho < \rho_c^*)$ and U_∞ $(\rho > \rho_c^*)$ increase as ρ increases in plane (ρ, p), and increase as p increases in plane (ρ, p). The planes are divided into functional $(P_\infty > 0, U_\infty > 0)$ and non-functional region$(P_\infty = 0, U_\infty = 0)$ by the red line. Here the white dashed line is the discontinuous phase transition threshold $p_c^I = 0.7741$ when there is no reinforced node $(\rho = 0)$, which is also the baseline of the phase transition compared to the equipped reinforced nodes $(\rho > 0)$. Further, the functional region is divided into non-collapse and recovery regions by the white dashed line. This division is to reflect the difference between not having reinforced nodes and having reinforced nodes, i.e., as the fraction of reinforced nodes increases from zero, the middle region changes from the original non-functional region $(P_\infty = 0, U_\infty = 0)$ to the functional region$(P_\infty > 0, U_\infty > 0)$, which is equivalent to the recovery region according to the network state. As a result, the plane is clearly divided into non-collapse, recovery, and collapse regions by the red line and the white dashed line.

As depicted in Figure C5(a) and Figure C5(b), with the decrease of p, for $\rho < \rho_c^*$, P_∞ is greater than zero when $p > p_c^I$, and drops discontinuously to zero at $p > p_c^I$; for $\rho > \rho_c^*$, P_∞ is greater than zero when $p > p_c^{II}\mid_{U_\infty}$, and drops continuously to zero at $p = p_c^{II}\mid_{U_\infty}$. In Figure C5(a) and Figure C5(b), with the increase of ρ, p_c^I and $p_c^{II}\mid_{U_\infty}$ gradually decrease, and the area of the collapse region becomes smaller. Note that when $p_c^I = p_c^{II}\mid_{U_\infty}$, we get the minimum reinforced fraction ρ_c^* that can keep the system from a catastrophic breakdown. After obtaining ρ_c^*, in order to further improve the reinforcement efficiency, the methods in these references [2–4] are adopted, which can better locate important nodes and reinforce them, and better enhance the system robustness.

Another important finding is that the area of the collapse region becomes smaller with increasing $\langle k\rangle$. Similarly, the area of the collapse region decreases with increasing α. These implicate that the system becomes more robust as the fraction ρ of reinforced nodes, the average degree $\langle k\rangle$, and the weak dependency parameter α increase. In addition, in Figure C5(c) and Figure C5(d), compared with the model with strong dependency links and reinforced nodes (SD-RN model) of reference [1], our model with weak dependency links and reinforce nodes(WD-RN model) is more robust and closer to the realistic scenario.

As shown in Figure C5, ρ_c^* is the minimum fraction of reinforced nodes to prevent the system from catastrophic breakdown. In Figure C6, the critical point ρ_c^* and the corresponding phase transition threshold p_c^* gradually decreases with the increase of α. The fraction $\rho = \rho_c^*$ of reinforced nodes represents the number of reinforcement devices arranged in each sub-network. The increase of the fraction of reinforced nodes implies that it is more expensive to arrange reinforcement devices in a real scenario, and therefore ρ_c^* represents the cost of reinforced devices. Although increasing the reinforcement devices can improve the system robustness and prevent system collapse, it comes at the expense of cost. In Figure C6, with the increase of weak dependence parameter α, the phase transition threshold p_c^* is smaller, and the system robustness is stronger. As the weak dependence parameter α increases, the minimum reinforced fraction ρ_c^* decreases, and the cost of equipping the reinforcement devices is reduced. Inspired by reference [5], considering the excessive cost of deploying reinforced nodes, this proposed model can realize the trade-off between high robustness and cost efficiency by tuning weak dependency parameter.

As shown in Figure C6(a) and Figure C6(b), the red line ρ_c^* divides the area into continuous phase transition region and discontinuous phase transition region. In Figure C6(c) and Figure C6(d), the discontinuous phase transition region gradually decreases with increasing $\langle k\rangle$. In particular, combining (C1), (C6), and (C11) together, for $\rho = 0$, we can get the maximum value $\alpha^*_{\max}$ of α_c^*. For ER-ER networks, when $\rho = 0$, combining Eqs. (C1), (C6), (C11), and (C8) together, we have

$$\langle k\rangle \left(\alpha^*_{\max}\right)^5 + 2\left(\alpha^*_{\max}\right)^2 - 2 = 0, \tag{C12}$$

where $\alpha^*_{\max}$ is only related to the average degree $\langle k\rangle$ and the value of $\alpha^*_{\max}$ decreases with increasing $\langle k\rangle$ in Figure C6(c) and Figure C6(d).

In the same way, for ER-ER networks, ρ_c^* reaches a maximum value ρ^*_{max} at $\alpha = 0$, which leads to

$$\rho^*_{\max} = 1 - \frac{\sqrt{e}}{2} \approx 0.1756, \tag{C13}$$

where ρ^*_{max} is a constant 0.1756 regardless of the average degree $\langle k\rangle$ in ER-ER networks. In SF-SF networks, one unanticipated finding was that the value of $\rho^*_{\max}$ decreases with increasing $\langle k\rangle$. As discussed above, a deeper insight is that when the parameter α (or ρ) is unknown, $\rho^*_{\max}$ (or $\alpha^*_{\max}$) is the upper bound of the minimum reinforced fraction ρ_c^* (or the minimum weak dependency parameter$\alpha^*_{\max}$) to prevent a catastrophic collapse of the system.

Appendix D Test on empirical networks

We testify our model in smart power grid of the Western States of the US, with the introduction of weak dependency links and a small density of reinforced nodes. A smart power grid consists of two networks: the power grid (PG) and autonomous systems of the Internet (AS), which are interdependent. Here, the US power grid consists of 4941 nodes, where the nodes can be a generator, transformer or substation, and the edges represents a power supply line [6]. The Internet autonomous system consists of 6474

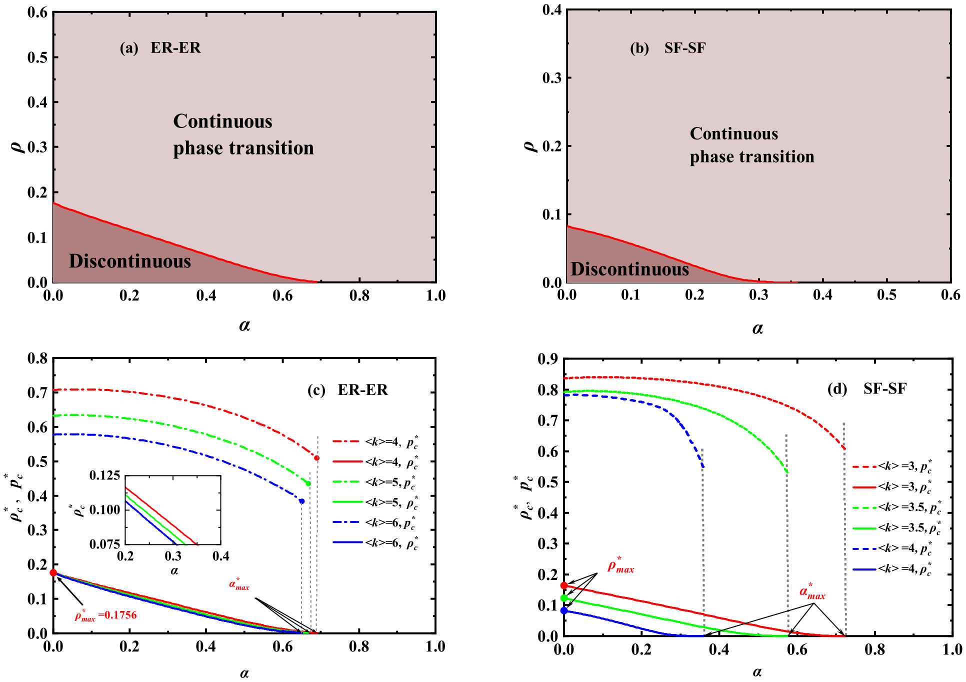

Figure C6 The critical threshold p_c^* and ρ_c^* as a function of weak dependency parameter α. In (a) and (b), the red line ρ_c^* divides the area into continuous phase transition region (light brown area) and discontinuous phase transition region (dark brown area). (a) ER-ER networks: $\langle k \rangle = 4$, (b) SF-SF networks: $\langle k \rangle = 4$, $\lambda_A = \lambda_B = 2.6$, $k \in [2, 1000]$. (c) In ER-ER networks, p_c^* and ρ_c^* as a function of α for different the average degree $\langle k \rangle$. (d) In SF-SF networks, p_c^* and ρ_c^* as a function of α for different the average degree $\langle k \rangle$. These lines are the theoretical results obtained by solving (C1), (C6), and (C11).

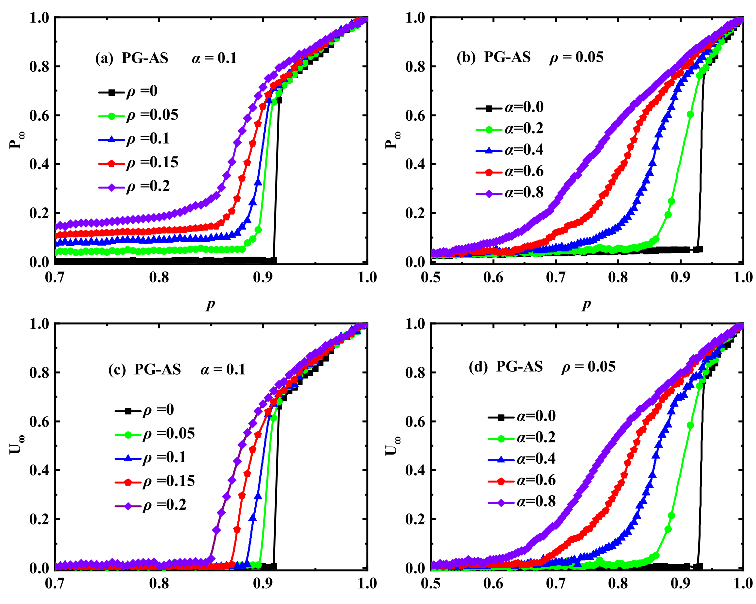

Figure D1 Percolation transition in the power grid of the western states of the US. (a) and (c): Simulation results of the P_∞ and U_∞ in PG-AS system as a function of p for different ρ with $\alpha = 0.1$. (b) and (d): Simulation results of the P_∞ and U_∞ in PG-AS system as a function of p for different α with $\rho = 0.05$. All simulation results are averaged over 100 realizations on networks.

nodes, where the nodes represent autonomous systems and the edges denote communication [7]. In each sub-network, a fraction ρ of nodes is randomly chosen as reinforced nodes, such as backup generators in the PG and Local Area Network in the AS. Due to the lack of data, the interdependent relationships between the PW and AS networks could not be captured directly. However, to gain qualitative insight into the issue, we take reasonable assumptions to construct interdependent networks, which can be considered as an approximation to many real-world networks. Here, there are more nodes in AS network than nodes in PG network, but it does not affect the failure mechanism of the whole network and can be ignored. We randomly choose 4941 nodes from the AS as counterparts of the nodes in the PG and establish a one-to-one interconnection (i.e., weak dependency link) between them, which represents the interaction of power and communication services between them. According to the assumptions of our model, when a node in the PG fails, each connectivity link of its dependency partner in the AS is disconnected from its neighbor nodes with a probability $1-\alpha$, and vice versa.

Figure D1 shows P_∞ and U_∞ as a function of p for different ρ and α in PG-AS networks. In Figure D1(a) and Figure D1(c), fixed $\alpha = 0.1$, we find that rich phase transition behavior by tuning the fraction ρ of reinforced nodes. As described in Figure C1, forρ less than a certain critical value ρ_c^*, the system undergoes an abruptly discontinuous phase transition for P_∞ and U_∞. For ρ greater than a certain critical value ρ_c^*, P_∞ is continuous and free from phase transitions and U_∞ is continuous phase transition. Similarly, in Figure D1(b) and Figure D1(d), fixed $\rho = 0.05$,we find that rich phase transition behavior by tuning weak dependency parameter α. According to the structural features of the real-world networks, we reasonably adjust the reinforced fraction and dependency strength to further significantly improve the robustness of the system while optimizing the resource allocation.

References

1 Yuan X, Hu Y Q, Stanley H E, et al. Eradicating catastrophic collapse in interdependent networks via reinforced nodes. Proc Natl Acad Sci USA, 2017, 114: 3311–3315
2 Zhao J, Wen T, Jahanshahi H, et al. The random walk-based gravity model to identify influential nodes in complex networks. Inf Sci, 2022, 609: 1706-1720
3 Wang C, Ma L L, Ma L, et al. Identification of influential users with cost minimization via an improved moth flame optimization. J Comput Sci, 2023, 67: 101955
4 Wen T, Gao Q Y, Chen Y W, et al. Exploring the vulnerability of transportation networks by entropy: A case study of Asia–Europe maritime transportation network. Reliab Eng Syst Saf, 2022, 226: 108578
5 Gao C, Fan Y, Jiang S H, et al. Dynamic robustness analysis of a two-layer rail transit network model. IEEE trans Intell Transp Syst, 2022, 23: 6509-6524
6 Watts D J, Strogatz S H. Collective dynamics of 'small-world'networks. Nature, 1998, 393: 440-442
7 Zhang B C, Liu R, Massey D, et al. Collecting the Internet AS-level topology. ACM SIGCOMM Comput Commun Rev, 2005, 35: 53-61
8 Feng L and Monterola C P and Hu Y Q. The simplified self-consistent probabilities method for percolation and its application to interdependent networks. New J Phys, 2015, 17: 063025